Characterizing Forest Fires Risks Using Free Multi-Source Data: Identifying High-Risk Road Sections

Gabriel E. Suárez-Fernández [1], Joaquín Martínez-Sánchez [1], Pedro Arias [1], Henrique Lorenzo[1]

[1] CINTECX, Universidade de Vigo. Applied Geotechnologies Group, Vigo, 36310, Spain – (gabrieleduardo.suarez, joaquin.martinez, parias, hlorenzo)@uvigo.gal

Keywords: LiDAR, Satellite Image, Forest Fire, Transport Infrastructure, Remote Sensing.

Abstract:

Transport infrastructures (TIs) play a crucial role for facilitating transportation and enhancing mobility. Nevertheless, they face significant risks from forest fires mainly due to climate change. Developing accurate fire risk maps is essential for planning vegetation maintenance, predicting fire-prone areas, and assessing potential damage levels. Risk maps often rely on field data, which are difficult to update promptly for effective management. This paper introduces an approach to identify and continuously monitor road sections at high risk of forest fires using Random Forest (RF) models along with satellite images. Multiple models were trained using different risk predictors, all achieving test accuracies exceeding 79% and good agreement in the kappa coefficient. Additionally, the key predictors in each model were analyzed. As a result, these models offer a dynamic updating mechanism for risk maps over time. The methodology also enables the integration and fusion of multi-source datasets to pinpoint areas with the highest risk associated with TIs and forest fires. These insights facilitate the delineation and timely update of critical TI areas, thereby enhancing overall risk management.

1. Introduction

The Sustainable Development Goals (SDGs) are a global initiative to eliminate poverty, preserve the environment, and enhance the well-being and future prospects of individuals worldwide. Constructing safe, sustainable, and resilient infrastructure, including regional and cross-border infrastructure, is essential to achieve territorial structuring, social cohesion, and equal opportunities.

Transport infrastructures (TIs) are currently a fundamental factor for the development of countries. Its conservation and the preservation of an optimal condition is necessary to guarantee the correct running of transport and economy. Nevertheless, the correct conservation and operation of this type of infrastructure is a challenge, since it is subject to a series of associated risks that jeopardize the safety of people on roads and the infrastructure itself (Rúa et al., 2022). One of the risks with the highest relevance is related to forest fires. Although it is not the only one, it has become more relevant in recent years due to the effects of climate change (Gajendiran et al., 2024).

The rising density of road networks near forested, shrubland, and grassland areas has significantly influenced the patterns of fire disturbance (Ricotta et al., 2018). These roads offer access that has both expanded the scope and efficiency of fire suppression efforts and established fire breaks that influence the spread of fires (Narayanaraj & Wimberly, 2011). However, the advantages that roads provide for fire prevention and management also come with associated risks, as increased road access has led to a higher frequency of human-caused ignitions in certain regions (Zambon et al., 2019).

The risk is defined as "(1) the hazard of a latent damaging event to the infrastructure, (2) the susceptibility of the elements and the environment, and (3) the values of the elements susceptible to loss" (Jactel et al., 2012). Therefore, creating fire risk maps is crucial for strategizing vegetation maintenance actions. The process of susceptibility mapping involves identifying areas where a forest fire is probable to happen, while the vulnerability mapping process assesses the potential level of damage that could result from forest fire (Chuvieco et al., 2023). Nevertheless, these maps often incorporate data taken in the field, which provide detailed information but cannot be easily updated (Domingo et al., 2020; Novo et al., 2020a).

Regular updates to forest fire risk maps are essential for effective management, as one of the primary contributors to fire ignition and spread is the surrounding vegetation (Molina et al., 2017), which undergoes significant changes over time (García-Cimarras et al., 2021). Both the condition and spatial distribution of vegetation play critical roles in defining fuel patterns (Abdollahi & Yebra, 2023), influencing risk assessment. Additionally, to fully grasp the potential hazard of an area, it is crucial to consider additional factors such as topography, meteorological conditions, and fire history (Abedi Gheshlaghi, 2019; Kayet et al., 2020; Novo et al., 2020b). Integrating these elements provides a comprehensive understanding of the forest fire risks, allowing for more accurate planning of preventive and response measures.

Remote Sensing (RS) technologies are extensively utilized as a method to assess vegetation health and safety (Van Pham et al., 2023), to identify alterations in land cover (De Luca et al., 2022; Nicolau et al., 2021; Seyam et al., 2023), to categorize fuel types (Domingo et al., 2020), and to identify forest fires (Suárez-Fernández et al., 2023). On the one hand, LiDAR (Light Detection and Ranging) is an active RS technology that proves invaluable in describing terrain and forest geometry (Aragoneses et al., 2024). It offers both horizontal and vertical information at exceptionally high spatial resolutions and accuracies (Castaño-Díaz et al., 2017). Nevertheless, the low temporal resolution prevents continuous follow-up over time and across years (Pirotti, 2011). On the other hand, satellite images from Landsat or Sentinel missions enable continuous and prolonged monitoring over time (Cartus & Santoro, 2019). Although, they also encounter constraints. These include the requirement for clear skies for multispectral images (Tian et al., 2023) or restricted capability to penetrate dense vegetation canopies for both multispectral and SAR images (Santoro et al., 2019, 2021). As a result, this study aims to identify and monitor road sections with the highest risk of forest fires. The risks associated with the physical environment and vegetation during a specific period will be characterized using publicly available data, such as LiDAR-PNOA and satellite technology. The resulting maps will be used to train Random Forest (RF) models, linking risks to satellite images. The main novelty lies in the generation of these risk maps

using only satellite technology over road infrastructures, which will allow continuous monitoring and update of the stretches over time.

2. Study Area and Materials

The study area is located in Northwest Spain, specifically in Pontevedra province, and covers four municipalities, as shown in Figure 1. This location is selected since it was classified as a critical area in terms of fire and landslides by Rúa et al. (2022). Among TIs analyzed include the Rías Baíxas A-52 highway, as well as the state routes N-120 and N-559.

Regarding materials, they are either freely available or in the public domain. The LiDAR data used in this study is sourced from the Spanish National Center for Geographic Information, dated July 2015, with a density of 0.5 points per square meter. As for satellite images, a combination of data from Landsat and Sentinel missions is utilized. Sentinel-1 provides images in the C-band of the Radar spectrum, while Sentinel-2 offers high-resolution optical images. The Landsat mission also provides optical images, but with lower spatial resolution than Sentinel-2. However, these satellites include a thermal band in the infrared spectrum. Both Sentinel-1 and Landsat thermal images are acquired using Google Earth Engine (GEE) platform (https://earthengine.google.com/), selecting the mean value for the last year prior to the dates of the Sentinel-2 images. Sentinel-2 images are downloaded from Copernicus Open Access Hub site (https://dataspace.copernicus.eu/), specifically selecting Level-2A data for both April 30, 2016, corresponding to the next spring season relative to the LiDAR-PNOA acquisition, and for April 18, 2024, representing the most recent spring season. For remaining data, Digital Terrain Model (DTM) and anthropogenic infrastructure data are sourced from the Spanish National Center for Geographic Information (https://centrodedescargas.cnig.es/CentroDescargas/index.jsp). Weather-related information includes the Historical Fire Weather Index (FWI) from NASA's Center for Climate Simulation (https://www.nccs.nasa.gov/) and Historical Fire Regimes from Suárez-Fernández et al. (2023).

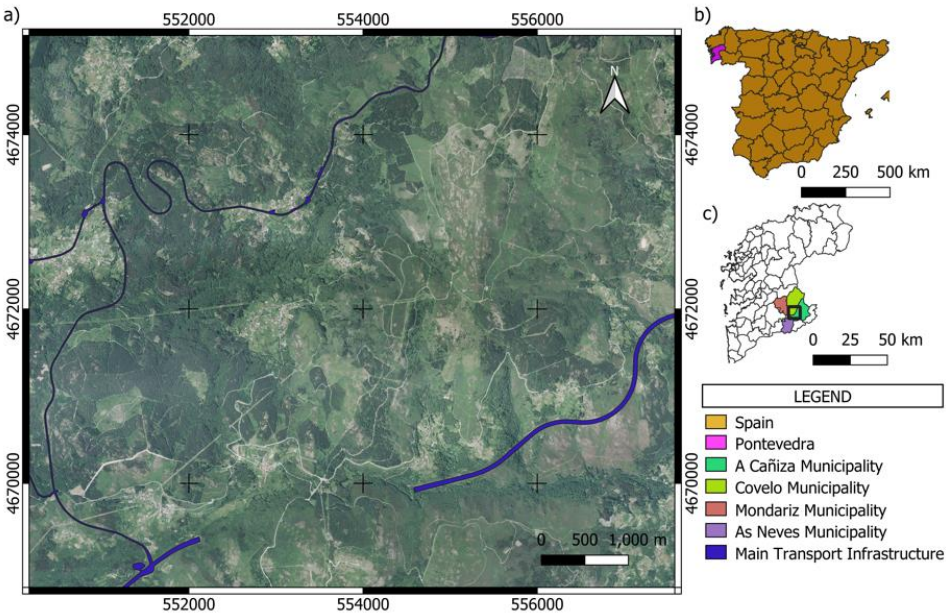

Figure 1. Study Area Overview. a) Main Transport Infrastructures to Study (coordinate system EPSG: 25829). b) Location of Galicia in the Spanish Territory. c) Study Area Location within Provinces.

3. Methodology

The overall methodology adopted to achieve the objective of this study is illustrated in Figure 2, which consists of four phases: Firstly, a pre-processing of LiDAR data. Secondly, the generation of layers for each parameter with associated risks in relation to forest fires issues. Thirdly, risk classification for each of these layers, followed by their fusion and integration to obtain general risks. Lastly, updating the maps generated to present-days, and verification and visualization of these resulting layers.

The pre-processing of LiDAR data involves the generation of several digital models necessary for the characterization of variables mainly related to vegetation. During the generation of layers, those parameters that have an inherent risk associated with forest fires issues are selected, followed by the obtention of their spatial distribution. This stage encompasses the consideration of vegetation-related variables, such as continuity, as well as fuel types, which are extracted from previously processed LiDAR data. Elements from the physical environment—such as geomorphology, meteorology, and human settlements—are taken into account, alongside historical fire data, the Fire Weather Index (FWI), and land use due to their significance in forest fire risk issues.

In the third phase, each layer is classified with a risk index ranging from 1 (very low) to 5 (very high). After creating the aforementioned layers, the hierarchy process is computed to determine the impact of each variable on the comprehensive risk map of the study area, using a vector of weights from Novo et al. (2020b). Subsequently, the preceding layer is integrated with the risk areas proximate to TIs, considering vegetation presence and continuity as a fundamental factor and its distance from roads, in compliance with current legislation (Xunta de Galicia, 2007). This integration results in the

production of the final fire risk map for TIs in the acquisition year of the LiDAR data.

Finally, an update of these risk maps is performed by training RF models that allows tracking of parameters with high temporal variability, such as vegetation. This phase allows bridging the time gap between the LiDAR-PNOA data and the present day. A verification of results is also carried out.

3.1 LiDAR-PNOA Data Pre-processing

A local data processing is developed using FUSION / LDV (version 4.41), which was developed by the US Forest Service for the analysis of LIDAR data. In this section, the LiDAR data are prepared to obtain statistics and to filter, describe and analyze the different types of vegetation in the study area.

Firstly, the Digital Elevation Model of Vegetation is obtained. The height of the ground at each return point is extracted using the DTM. As a result, the model of the height of each return point above ground is acquired. Valid points belonging to vegetation are then filtered out, excluding human settlements, roads, or any anthropogenic infrastructure.

Subsequently, a 30x30m grid is created, and statistics are calculated for each of them, stratifying the statistics according to the type of vegetation as shown in Table 1. The grid size is crucial since a very small value would result in a loss of returns, increasing the error due to inconsistency and unreliability. In contrast, a very large grid size would reduce the accuracy in the relationship between statistics and terrain, as well as being subject to the edge effect, resulting in lower accuracy.

Vegetation layer	Height Range	
	Minimum	Maximum
Medium Vegetation	0.5m	2m
Medium-High Vegetation	2m	4m
High Vegetation	4m	55m
Total Vegetation	0.5m	55m

Table 1. Vegetation Layer Classification

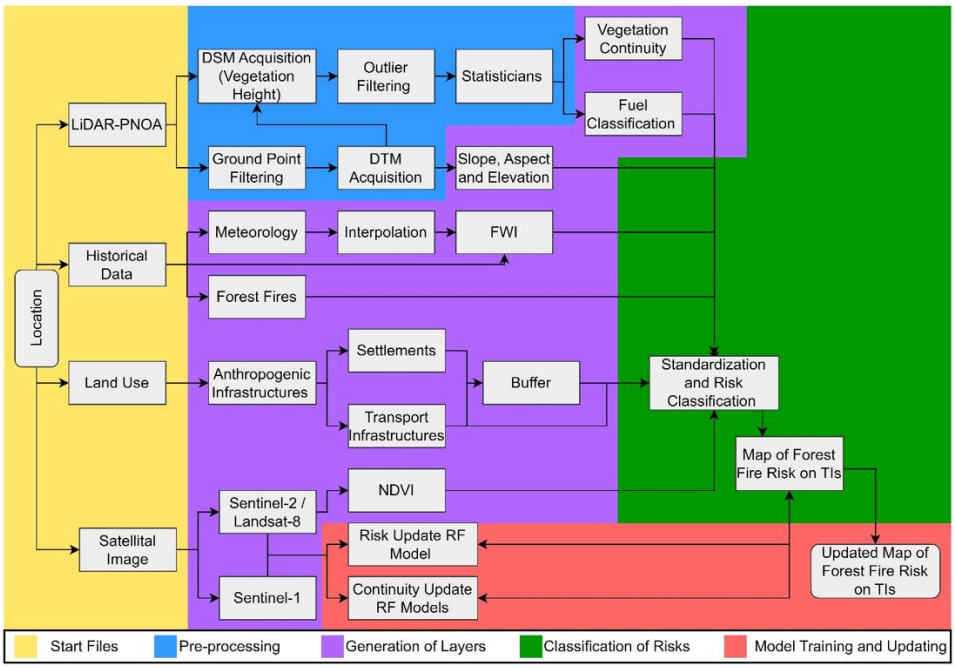

Figure 2. Workflow of Methodology.

3.2 Obtaining Predictors

The various variables that influence risk, both for the total area and for the main TIs, are quantified, classified, and normalized. These variables are divided into two main groups. The first group involves collecting and extracting the necessary variables to create a cartography showing forest fire risk throughout the study area. This includes historical analyses, settlement distances, geomorphology, forest fuels, Normalized Difference Vegetation Index (NDVI) and meteorological indices, as detailed in Abedi Gheshlaghi, (2019) and Kayet et al. (2020). The second group focuses on vegetation continuity and compliance with minimum safety distances on national transportation routes, as shown Novo et al., 2020a). The combination of these groups will allow for the identification of the most critical road section within the selected location.

3.2.1 Vegetation

Vegetation classification is carried out by characterizing the fuel models, following the Prometheus system, adapted from the Northern Forest Fire Laboratory (NFFL) for Mediterranean conditions (Albini, 1976; Domingo et al., 2020). This process is performed according to Table 2, which provides statistics to determine the coverage of the different strata and the average heights in each grid cell. The Fractional Green Canopy Cover (FGCC), which is equivalent to the percentage of first returns of the point cloud, is calculated along with the average height.

Assessing the state and condition of vegetation is essential. The NDVI, which provides valuable insights into its health is used for that. This parameter is derived from Sentinel-2 files, synchronized with the season of LiDAR data acquisition.

Fuel Type	Cover	Shrub Height	ΔShrubs/ Trees
FT1	>60% grass		
FT2		0.3-0.6m	
FT3	>60% shrubs and <50% trees	0.6-2.0m	
FT4		2.0-4.0m	
FT5	<30% shrubs and >50% trees		
FT6	>30% shrubs and >50% trees		>0.5m
FT7			<0.5m

Table 2. Fuel types defined by the Prometheus classification. Extracted from Domingo et al. (2020)

3.2.2 Topography

The terrain geomorphology is characterized by three main variables: elevation, aspect, and slope. Elevation corresponds to the DTM data itself, while aspect and slope are derived using the GDAL library in QGIS software (version 3.16.9). The files are then adjusted to match the 30m grid cells, simplifying their integration and analysis with other variables.

3.2.3 Meteorological Conditions

The Historical Fire Weather Index (FWI) is utilized, comprising six sub-indices, with the FWI serving as the final index. This index considers the humidity of dead fuels in the soil and subsoil, as well as the wind effect, to produce an indicator estimating fire spread intensity. A total of 420 files containing FWI data at a global level are obtained, and their arithmetic mean is calculated. This yields the average value of this index for the summer period over the last 35 years.

3.2.4 Anthropogenic Infrastructures and Forest Fires Record

Using data from roads and population settlement, various areas of influence are determined using a buffer tool in QGIS software. This process categorizes areas based on the type of structure, distinguishing between linear infrastructure (roads) and other structures (settlements). Concerning forest fire history, both the recurrence and the time elapsed since the last recorded fire (TSF) are obtained from the fire database.

3.2.5 Vegetation Continuity

The FGCC is defined as the degree of plot coverage by vertical projection of the tree canopy onto it. For this study, considering a grid size of 30x30m, the FGCC is determined as the percentage of LiDAR first returns captured by vegetation within the analyzed height range and the specified strata (as section 3.2.1), which defines the horizontal continuity.

As for vertical continuity, it pertains to the presence of vegetation distributed vertically in a continuous and uniform manner. To describe this continuity in the study area, the Canopy Relief-Ratio (CRR) ratio (Parker & Russ, 2004), as defined by Equation 1, is utilized. The CRR is calculated as a statistic that relates to the free canopy length of the stand based on height observations. This parameter ranges from 0 to 1, with values below 0.5 indicating that most of the biomass is in the lower parts, while values above 0.5 indicate that most of the biomass is in the canopy.

$$CRR = \frac{Height_{mean} - Height_{minimum}}{Height_{maximum} - Height_{minimum}} \quad (1)$$

3.3 Risk Map for Input Data

The predictors are then normalized by assigning values ranging from 1 (very low) to 5 (very high), according to established classes. Subsequently, they are grouped to determine the total risk of the study area on the same scale from 1 to 5. For both processes, the weightings and ranges developed by Novo et al. (2020b) for the region of Galicia are used, resulting in the total fire risk (FR).

The areas that affect or have a greater influence on the TIs are also delimited. This is achieved by detecting areas that do not comply with applicable legislation on forest fire prevention (Xunta de Galicia, 2007), which establishes a horizontal vegetation clearance of 4m or 10m, depending on the type of species. The most restrictive limitation (10m) is used to identify tree species.

Finally, CRR values between 0.33 and 0.66 are selected, which indicate a homogeneous distribution of biomass. To identify the kilometer points with the highest vulnerability, the areas with vertical continuity are combined with those that do not comply with the required safety distances, and these are intersected with the areas with the highest FR (> 4). What it boils down to is that the most critical points or areas are determined by combining factors from the physical and vegetation environment, enabling an evaluation of the overall risk of the location. The identification of areas with extreme risk, along with cells that present vertical continuity and those that lack safety distance, allows for the delineation of critical areas and the determination of the points with the greatest risk to TIs.

3.4 Random Forest Model Training and Testing

The map update is essential due to considerable temporal discontinuity in the LiDAR data provided by the PNOA, dating back to 2015. Possible variations among the data, maps obtained, and the current situation could be significant, especially due to changes in the vegetation for natural or anthropogenic reasons. Therefore, Sentinel satellite images from 2015 (see Section 2) are used to train RF models, incorporating vegetation indices or proxy variables detailed in Table 3. These models aim to identify and classify the several risks presented by maps obtained previously, such as FR, CRR and species identification.

For both FR and CRR, the 30m grid tiles previously obtained are used as training and validation data, adjusting the pixel size of the satellite image, for which the mean value is used. In contrast, to identify trees in the safety buffer areas, a grid cell size matching the Sentinel bands of higher resolution (10m) is used, assigning the presence or absence of trees according to the height of the LiDAR points.

The RF models are trained using RStudio/2022.12.0 (R language version 4.1.3), splitting the data with an 80/20 partition. The models are then evaluated using both the confusion matrix and the Kappa coefficient. The Kappa coefficient measures the agreement between predictions and observations, adjusting model performance relative to random expectations. Importance measures of the variables are also incorporated to assess their significance, helping to identify the most influential variables in the classification.

Finally, the trained models are applied to the current satellite image to identify critical sections of TIs. These sections are then visually evaluated in the field to confirm the accuracy of the identification.

Index or Proxy	Equation
NDVI	$\frac{NIR - RED}{NIR + RED}$
EVI	$\frac{2.5 * (NIR - RED)}{(NIR + 6 * RED - 7.5 * BLUE) + 1}$
SAVI	$\frac{NIR - RED}{NIR + RED + L} * (1 + L) \quad L = 0.5$
ARVI	$\frac{NIR - 2 * RED + BLUE}{NIR + 2 * RED + BLUE}$
GCI	$\frac{NIR}{GREEN} - 1$
SIPI	$\frac{NIR - BLUE}{NIR - RED}$
NBR	$\frac{NIR - SWIR}{NIR + SWIR}$
VIN	$\frac{NIR}{RED}$
WDRVI	$\frac{0.1 * NIR - RED}{0.1 * NIR + RED}$
SI1	$VH + VV$
SI2	$VV - VH$
SI3	$VH - VV$
SI4	$VH * VV$
SI5	VH/VV
SI6	VV/VH
SI7	$\frac{VV + VH}{2}$
SI8	$\sqrt{VV - VH}$

Table 3. Sentinel-2 vegetation indices and Sentinel-1 proxy variables derived as predictors.

4. Results

This section presents key results derived from LiDAR processing, data analysis, and modeling, leading to the creation of current risk maps. The results are organized according to the methodology, starting from the generation of LiDAR-PNOA risk maps, followed by RF models training and assessment, and concluding with the generation of the current risk map.

4.1 Risk Map as Input Data

The generation of the base maps required calculating and normalizing a set of biophysical variables. In relation to meteorological conditions, variations within the study area were not deemed relevant. Therefore, a constant and normalized value of 3 was assigned to the FWI, obtained from the corresponding historical data (see Section 3.2.3). Finally, each map was transformed to a scale from 0 to 1, as shown in Figure 3, based on the established criteria (see Section 3.3), where a value of 1 was assigned to the cells with the highest associated risk.

4.2 RF Models

The three RF models for updating risk maps demonstrated different levels of performance in each case. For the overall risk maps, which encompass both vegetation-related biotic variables and physical variables of the environment, an accuracy of 80.27% was achieved in the test, with a 95% confidence interval (CI) ranging from 79.49% to 81.03%. The kappa coefficient was 0.4991. As for the second model, designed to identify vertical continuity from the CRR, the accuracy decreased slightly, reaching 79.74% in the test, with a CI ranging from 78.96% to 80.51%. The kappa value increased significantly to 0.5767. Finally, in the vegetation detection model, where a grid size of 10m was used to increase the spatial resolution, an accuracy of 90.14% was obtained in the test, with a CI ranging from 89.46% to 90.80%. The kappa value for this model also increased to 0.8017, reaching an almost perfect concordance. Regarding the ROC curves, all three models showed an area under the curve (AUC) greater than 85%, as depicted in Figure 4.

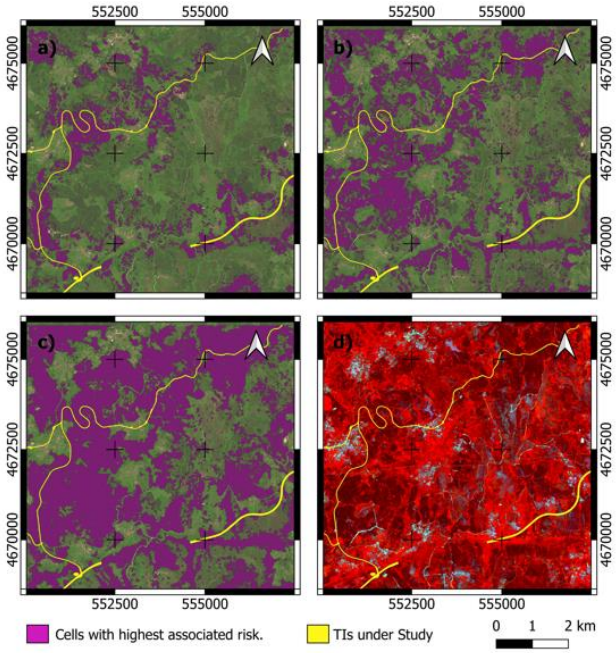

Figure 3. Risk Maps for Input Data (coordinate system EPSG: 25829). a) Highest Fire Risk Map b) Homogeneous Vertical Distribution of Biomass Map. c) High Vegetation Presence Map. d) Sentinel Infrared Visualization

The importance of the predictors was assessed using Mean Decrease Accuracy and the Mean Decrease Gini. Figure 5 shows the results of Mean Decrease Accuracy for the 25 most important predictors in each model. In the fire risk RF model, the first five predictors comprise mainly factors related to the physical environment, such as altitude, aspect, and distances to anthropogenic infrastructure, along with the thermal band. In the vertical continuity model, the top five predictors include exclusively satellite bands from both Sentinel-1 and Sentinel-2, while for the vegetation identification model, the five most important variables are oriented towards a combination of bands with proxy variables from both satellite sources.

4.3 Final Current Maps

Finally, using the trained models and the year 2024 Sentinel multispectral image (see section 2), together with the corresponding Landsat and Sentinel-1 mean value images from the prior year, the updated risk maps were generated, as shown in Figure 6. These areas were then surveyed in the field.

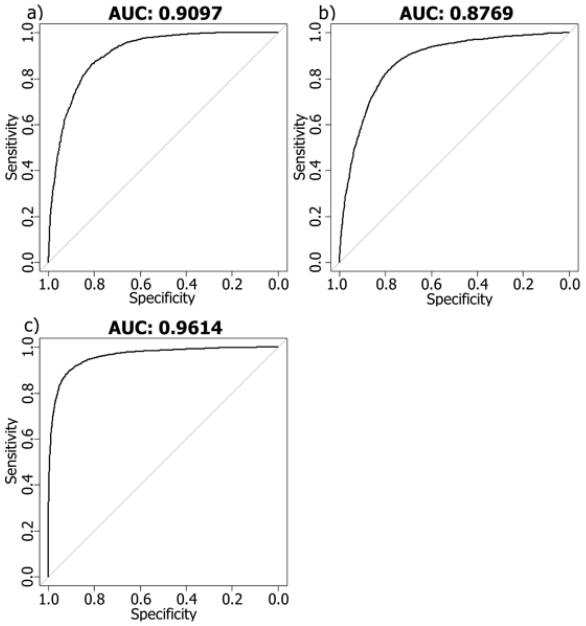

Figure 4. ROC Curves. a) For Fires Risk Model. b) For Vertical Distribution Model. c) For High Vegetation Presence Model.

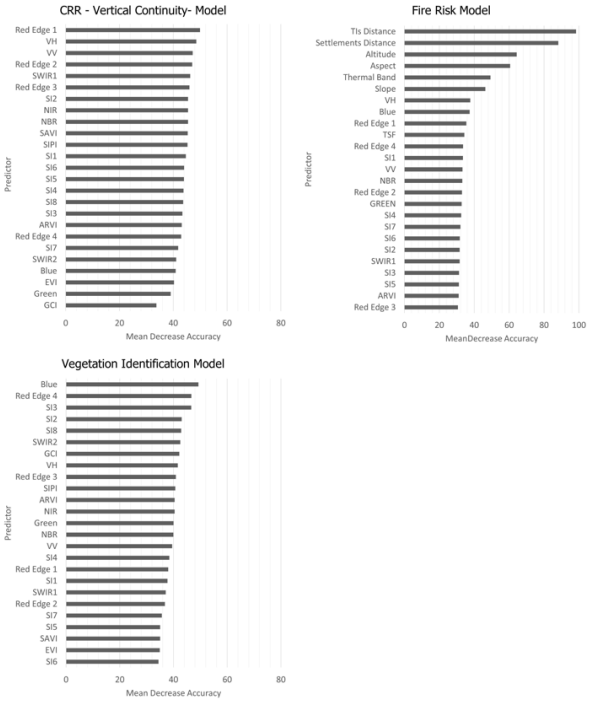

Figure 5. Importance of main predictors for each model.

5. Discussion

Different risk maps were obtained from open LiDAR-PNOA data to train several RF models using satellite images. As a result, different models were acquired. These models allowed the identification of tiles with a higher vulnerability level, caused by both continuity in vegetation and high FR. This facilitated the update of the maps for identifying critical sections. Therefore, this section analyzes and discusses the results obtained using the methodology developed.

In relation to the FR maps used as input to the models, they have been obtained through a methodology extensively used by several authors, such as Kayet et al. (2020) and Abedi Gheshlaghi (2019), emphasizing the weights of variables for our specific case study. The weights were those established by Novo et al. (2020b) for a place located in the same region. Regarding using LiDAR data as a basis for training models, this approach has been applied by Cartus & Santoro (2019) or Aragoneses et al. (2024), who from LiDAR-derived metrics, generated biomass maps. These maps were subsequently used to calibrate the models that allowed defining that variable from reflectance or backscattering values. In this study, this approach was adopted, using several LiDAR-derived metrics to obtain the critical tiles required to adjust the RF models.

Concerning limitations in this approach, they were mainly characterized by two key factors. The first factor was the low density of point clouds provided by LiDAR-PNOA (0.5 pts/m²), which often results in a scarcity of points. Even though these low densities can estimate structural attributes, as shown in Castaño-Díaz et al. (2017), the lack of points could hinder an accurate characterization of forest stands, which was demonstrated by Estornell et al. (2011). The second limitation was the temporal discontinuity of LiDAR-PNOA data, dating back to 2015 (the last available coverage). Although models have been developed to address this limitation, periodic updating of LiDAR is essential to detect subtle changes in the physical and biological environment that may not be evident in satellite images, as illustrated in Rada et al. (2022).

It is crucial to highlight the influence and predictive capacity of certain satellite sensors, depending on the response analyzed. This relevance was determined by the weights of the predictors in the RF models, as depicted in Figure 5. Unlike Kayet et al. (2020) or Seyam et al. (2023), which relied exclusively on multispectral satellite images, or Santoro et al. (2021), which used SAR technology, this study integrated several satellite imaging technologies to analyze the state of vegetation, following the approach shown by Van Pham et al. (2023). Both multispectral and SAR images from Sentinel and Landsat missions were used to identify vulnerable tiles and, as a result, critical stretches on the TIs. In the RF model for the FR, the combination of predictors covering biotic and physical variables was highlighted, in line with the methodologies that supported the obtaining of these maps. Regarding the CRR model, the most relevant predictors included the combination of multispectral and SAR images, taking advantage of SAR's canopy penetration capability. In contrast to the findings of Santoro et al. (2019), where the suitability of Sentinel-1 C-band for quantifying log volume was questioned, our study demonstrated the suitability of that band for estimating CRR. Finally, in terms of predictors for tree identification, the combination of multispectral bands with Sentinel-1 proxies stood out. This agrees with Nicolau et al. (2021), who concluded that the use of dual polarimetric SAR indices (VV and VH), improve spectral separability among cover classes. Nevertheless, De Luca et al. (2022) found that the contribution of backscattering in the C-band is not as decisive as that in some optical bands. Consequently, this approach should be validated in different study areas.

Therefore, training and implementation of the RF models using satellite images enabled the modeling of the spectral response of various factors that increase risk or vulnerability. As a result, this process significantly facilitated the update of the tiles and, consequently, of the critical sections, since the models are applicable to satellite images obtained in any given year.

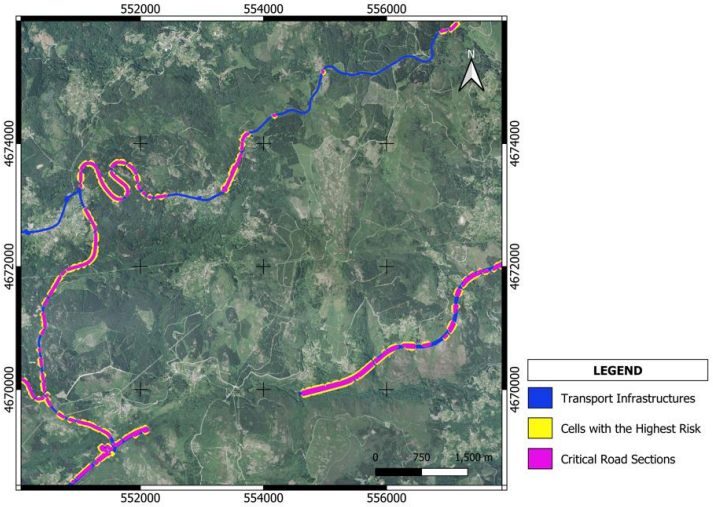

Figure 6. Critical Road Sections Over Transport Infrastructure for the Current Year (coordinate system EPSG: 25829).

6. Conclusions

This study presented a methodology for identifying and updating road sections with the highest risk of forest fires. Based on the LiDAR statistics, forest fire risk maps were generated. Despite technical limitations, such as low density of points or temporal discontinuity, the generated maps allowed identifying vulnerable sections. Integrating multi-sensor satellite images with these risk maps achieved significant accuracies in risk detection using RF models. Therefore, the methodology allowed for the integration and fusion of multi-source datasets. This enabled the identification, in a cost-effective and straightforward manner, of sections with the highest associated risk concerning TIs and forest fires. These findings facilitate the delineation and update of critical TI areas, improving risk management. Thus, future research should focus on the identified road segments, with an emphasis on capturing denser point clouds and assessing the applicability of the C-band in other regions. This approach could provide a more accurate description of forest stands.

Acknowledgements

This study was supported by "Ayudas para la Formación de Profesorado Universitario (FPU)", Government of Spain [FPU21/03038]. The work is part of the TED2021-132000B-I00 project, funded by MCIN/AEI/10.13039/501100011033 and European Union "NextGenerationEU"/PRTR".

References

Abdollahi, A., & Yebra, M. (2023). Forest fuel type classification: Review of remote sensing techniques, constraints and future trends. In *Journal of Environmental Management* (Vol. 342). Academic Press. https://doi.org/10.1016/j.jenvman.2023.118315

Abedi Gheshlaghi, H. (2019). Using GIS to Develop a Model for Forest Fire Risk Mapping. *Journal of the Indian Society of Remote Sensing*, *47*(7), 1173–1185. https://doi.org/10.1007/s12524-019-00981-z

Albini, F. A. (1976). *Estimating wildfire behavior and effects* (Vol. 30). Department of Agriculture, Forest Service, Intermountain Forest and Range Experiment Station.

Aragoneses, E., García, M., Ruiz-Benito, P., & Chuvieco, E. (2024). Mapping forest canopy fuel parameters at European scale using spaceborne LiDAR and satellite data. *Remote Sensing of Environment*, *303*, 114005. https://doi.org/10.21950/KTALA8

Cartus, O., & Santoro, M. (2019). Exploring combinations of multi-temporal and multi-frequency radar backscatter observations to estimate above-ground biomass of tropical forest. *Remote Sensing of Environment*, *232*. https://doi.org/10.1016/j.rse.2019.111313

Castaño-Díaz, M., Álvarez-Álvarez, P., Tobin, B., Nieuwenhuis, M., Afif-Khouri, E., & Cámara-Obregón, A. (2017). Evaluation of the use of low-density LiDAR data to estimate structural attributes and biomass yield in a short-rotation willow coppice: an example in a field trial. *Annals of Forest Science*, *74*(4). https://doi.org/10.1007/s13595-017-0665-7

Chuvieco, E., Yebra, M., Martino, S., Thonicke, K., Gómez-Giménez, M., San-Miguel, J., Oom, D., Velea, R., Mouillot, F., Molina, J. R., Miranda, A. I., Lopes, D., Salis, M., Bugaric, M., Sofiev, M., Kadantsev, E., Gitas, I. Z., Stavrakoudis, D., Eftychidis, G., … Viegas, D. (2023). Towards an Integrated Approach to Wildfire Risk Assessment: When, Where, What and How May the Landscapes Burn. *Fire*, *6*(5). https://doi.org/10.3390/fire6050215

De Luca, G., M. N. Silva, J., Di Fazio, S., & Modica, G. (2022). Integrated use of Sentinel-1 and Sentinel-2 data and open-source machine learning algorithms for land cover mapping in a Mediterranean region. *European Journal of Remote Sensing*, *55*(1), 52–70. https://doi.org/10.1080/22797254.2021.2018667

Domingo, D., de la Riva, J., Lamelas, M. T., García-Martín, A., Ibarra, P., Echeverría, M., & Hoffrén, R. (2020). Fuel type classification using airborne laser scanning and sentinel 2 data in mediterranean forest affected by wildfires. *Remote Sensing*, *12*(21), 1–22. https://doi.org/10.3390/rs12213660

Estornell, J., Ruiz, L. A., Velázquez-Martí, B., & Fernández-Sarría, A. (2011). Estimation of shrub biomass by airborne

LiDAR data in small forest stands. *Forest Ecology and Management*, *262*(9), 1697–1703. https://doi.org/10.1016/j.foreco.2011.07.026

Gajendiran, K., Kandasamy, S., & Narayanan, M. (2024). Influences of wildfire on the forest ecosystem and climate change: A comprehensive study. In *Environmental Research* (Vol. 240). Academic Press Inc. https://doi.org/10.1016/j.envres.2023.117537

García-Cimarras, A., Manzanera, J. A., & Valbuena, R. (2021). Analysis of mediterranean vegetation fuel type changes using multitemporal lidar. *Forests*, *12*(3). https://doi.org/10.3390/f12030335

Jactel, H., Branco, M., Duncker, P., Gardiner, B., Grodzki, W., Langstrom, B., Moreira, F., Netherer, S., Nicoll, B., Orazio, C., Piou, D., Schelhaas, M. J., & Tojic, K. (2012). A multicriteria risk analysis to evaluate impacts of forest management alternatives on forest health in Europe. *Ecology and Society*, *17*(4). https://doi.org/10.5751/ES-04897-170452

Kayet, N., Chakrabarty, A., Pathak, K., Sahoo, S., Dutta, T., & Hatai, B. K. (2020). Comparative analysis of multi-criteria probabilistic FR and AHP models for forest fire risk (FFR) mapping in Melghat Tiger Reserve (MTR) forest. *Journal of Forestry Research*, *31*(2), 565–579. https://doi.org/10.1007/s11676-018-0826-z

Molina, J. R., Martín, T., Rodríguez Y Silva, F., & Herrera, M. Á. (2017). The ignition index based on flammability of vegetation improves planning in the wildland-urban interface: A case study in Southern Spain. *Landscape and Urban Planning*, *158*, 129–138. https://doi.org/10.1016/j.landurbplan.2016.11.003

Narayanaraj, G., & Wimberly, M. C. (2011). Influences of forest roads on the spatial pattern of wildfire boundaries. *International Journal of Wildland Fire*, *20*(6), 792–803. https://doi.org/10.1071/WF10032

Nicolau, A. P., Flores-Anderson, A., Griffin, R., Herndon, K., & Meyer, F. J. (2021). Assessing SAR C-band data to effectively distinguish modified land uses in a heavily disturbed Amazon forest. *International Journal of Applied Earth Observation and Geoinformation*, *94*. https://doi.org/10.1016/j.jag.2020.102214

Novo, A., Fariñas-álvarez, N., Martínez-Sánchez, J., González-Jorge, H., Fernández-Alonso, J. M., & Lorenzo, H. (2020b). Mapping forest fire risk—a case study in Galicia (Spain). *Remote Sensing*, *12*(22), 1–21. https://doi.org/10.3390/rs12223705

Novo, A., Fariñas-Álvarez, N., Martínez-Sánchez, J., González-Jorge, H., & Lorenzo, H. (2020a). Automatic processing of aerial LiDAR data to detect vegetation continuity in the surroundings of roads. *Remote Sensing*, *12*(10). https://doi.org/10.3390/rs12101677

Parker, G. G., & Russ, M. E. (2004). The canopy surface and stand development: Assessing forest canopy structure and complexity with near-surface altimetry. *Forest Ecology and Management*, *189*(1–3), 307–315. https://doi.org/10.1016/j.foreco.2003.09.001

Pirotti, F. (2011). Analysis of full-waveform LiDAR data for forestry applications: A review of investigations and methods. In *IForest* (Vol. 4, Issue JUNE, pp. 100–106). https://doi.org/10.3832/ifor0562-004

Rada, P., Padilla, A., Horák, J., & Micó, E. (2022). Public LiDAR data are an important tool for the detection of saproxylic insect hotspots in Mediterranean forests and their connectivity. *Forest Ecology and Management*, *520*. https://doi.org/10.1016/j.foreco.2022.120378

Ricotta, C., Bajocco, S., Guglietta, D., & Conedera, M. (2018). Assessing the influence of roads on fire ignition: Does land cover matter? *Fire*, *1*(2), 1–9. https://doi.org/10.3390/fire1020024

Rúa, E., Comesaña-Cebral, L., Arias, P., & Martínez-Sánchez, J. (2022). A top-down approach for a multi-scale identification of risk areas in infrastructures: particularization in a case study on road safety. *European Transport Research Review*, *14*(1). https://doi.org/10.1186/s12544-022-00563-0

Santoro, M., Cartus, O., & Fransson, J. E. S. (2021). Integration of allometric equations in the water cloud model towards an improved retrieval of forest stem volume with L-band SAR data in Sweden. *Remote Sensing of Environment*, *253*. https://doi.org/10.1016/j.rse.2020.112235

Santoro, M., Cartus, O., Fransson, J. E. S., & Wegmüller, U. (2019). Complementarity of X-, C-, and L-band SAR backscatter observations to retrieve forest stem volume in boreal forest. *Remote Sensing*, *11*(13). https://doi.org/10.3390/rs11131563

Seyam, M. M. H., Haque, M. R., & Rahman, M. M. (2023). Identifying the land use land cover (LULC) changes using remote sensing and GIS approach: A case study at Bhaluka in Mymensingh, Bangladesh. *Case Studies in Chemical and Environmental Engineering*, *7*. https://doi.org/10.1016/j.cscee.2022.100293

Suárez-Fernández, G. E., Martínez-Sánchez, J., & Arias, P. (2023). A NOVEL METHODOLOGY FOR THE AUTOMATIC ACQUISITION OF REAL FOREST FIRE DATASETS OVER LONG PERIODS OF TIME. *International Archives of the Photogrammetry, Remote Sensing and Spatial Information Sciences - ISPRS Archives*, *48*(1/W1-2023), 465–472. https://doi.org/10.5194/isprs-archives-XLVIII-1-W1-2023-465-2023

Tian, L., Wu, X., Tao, Y., Li, M., Qian, C., Liao, L., & Fu, W. (2023). Review of Remote Sensing-Based Methods for Forest Aboveground Biomass Estimation: Progress, Challenges, and Prospects. In *Forests* (Vol. 14, Issue 6). Multidisciplinary Digital Publishing Institute (MDPI). https://doi.org/10.3390/f14061086

Van Pham, T., Do, T. A. T., Tran, H. D., & Do, A. N. T. (2023). Assessing the impact of ecological security and forest fire susceptibility on carbon stocks in Bo Trach district, Quang Binh province, Vietnam. *Ecological Informatics*, *74*. https://doi.org/10.1016/j.ecoinf.2022.101962

Xunta de Galicia. (2007). Ley 3/2007, de 9 de Abril, de Prevencion y Defensa Contra los Incendios Forestales de Galicia. In *Boletin Oficial del Estado BOE* (Vol. 119, pp. 21377–21394).

Zambon, I., Cerdà, A., Cudlin, P., Serra, P., Pili, S., & Salvati, L. (2019). Road network and the spatial distribution of wildfires in the valencian community (1993–2015). *Agriculture (Switzerland)*, *9*(5). https://doi.org/10.3390/agriculture9050100